Polymer 49 (2008) 2937–2946

Contents lists available at ScienceDirect

Polymer

journal homepage: www.elsevier.com/locate/polymer

Adhesion of statistical and blocky ethylene–octene copolymers to polypropylene

P. Dias [a], Y.J. Lin [a], B. Poon [b], H.Y. Chen [b], A. Hiltner [a,*], E. Baer [a]

[a] Department of Macromolecular Science and Engineering and Center for Applied Polymer Research, Case Western Reserve University, Cleveland, OH 44106-7202, United States
[b] New Products – Materials Science, Core R&D, The Dow Chemical Company Freeport, TX 77541, United States

ARTICLE INFO

Article history:
Received 19 January 2008
Received in revised form 10 April 2008
Accepted 11 April 2008
Available online 28 May 2008

Keywords:
Delamination toughness
Olefin copolymers
Tie-layer

ABSTRACT

This study examined the effect of chain microstructure on the adhesion of ethylene–octene copolymers to polypropylene. The copolymers were candidates for compatibilization of polypropylene (PP) and high density polyethylene (HDPE) blends, and included a blocky copolymer, a statistical copolymer that had the same composition as the soft segment of the blocky copolymer, and a statistical copolymer that had the same comonomer content and crystallinity as the blocky copolymer. The compatibilized melt blend was modeled by a microlayered, one-dimensional structure consisting of alternating layers of PP and HDPE, each separated by a thin tie-layer. The microlayered structure made it possible to directly measure the adhesion using the T-peel test. Infrared analysis of matching peel fracture surfaces established that fracture occurred adhesively at the interface between PP and the tie-layer. Direct observation of the damage zone at the crack tip and microscopic examination of the fracture surfaces revealed that the tie-layer was highly deformed before final separation occurred at the interface. The substantially higher delamination toughness of the blocky copolymer compared to the statistical copolymers could be accounted for by considering both interspherulitic mechanically interlocking influxes and intraspherulitic entrapment of interdiffused tie-layer chains. The blocky copolymer also retained delamination toughness to a higher temperature due to the greater stability of lamellar crystals compared to fringed micellar crystals.

1. Introduction

Polypropylene (PP) and high density polyethylene (HDPE) are amongst the most abundantly used polymers due to their low cost, mechanical robustness, and melt processability. Blending the two materials could achieve properties that are not obtainable with the individual polymers. Unfortunately, the polymers are incompatible, and their blends show extremely poor toughness and tensile elongation properties. The performance properties of incompatible blends can be improved dramatically by the addition of a small amount of the appropriate compatibilizer, usually a opolymer. Early studies demonstrated that the compatibilization of polyolefin blends with low density polyethylene or ethylene–propylene rubber (EPR) substantially increased the elongation at break [1]. Since then, a variety of copolymers, including EPDM, EVA, SBS, and SEBS, have been studied, with EPDM proving to be the most effective for improving mechanical properties in uniaxial extension [2–7].

The most effective compatibilizers are composed of monomers or segments that are miscible or compatible with both phases. Their presence at the interface lowers the interfacial tension, reduces the particle size, and promotes adhesion between the two phases. Copolymer molecules cross the interface forming bridges that couple the two phases together. Among the various chain structures, diblock or triblock copolymers are the most widely used compatibilizers. Theoretical results suggest that blocky copolymers form more interfacial bridges than statistical copolymers [8,9]. An optimum advantage is achieved when the blocks are longer than an effective entanglement molecular weight of the block.

Recently, The Dow Chemical Company developed a chain shuttling catalyst technology that can be used to synthesize olefin block copolymers (OBC) in a continuous process [10]. The block copolymers synthesized by chain shuttling technology consist of crystallizable ethylene–octene blocks with very low comonomer content and high melting temperature, alternating with amorphous ethylene–octene blocks with high comonomer content and low glass transition temperature. The new blocky copolymers have a statistical multiblock architecture with a distribution in block lengths and a distribution in the number of blocks per chain.

As the OBC soft segment is expected to be compatible with PP and the hard segment is expected to be compatible with HDPE, OBC should be an excellent compatibilizer for PP/HDPE blends. Indeed,

* Corresponding author. Department of Macromolecular Science and Engineering and Center for Applied Polymer Research, Case Western Reserve University, 10900 Euclid Ave, Cleveland, OH 44106-7202, United States.
E-mail address: ahiltner@case.edu (A. Hiltner).

0032-3861/$ – see front matter © 2008 Elsevier Ltd. All rights reserved.
doi:10.1016/j.polymer.2008.04.022

a recent study demonstrated that an OBC was substantially more effective than a statistical copolymer in increasing the elongation at break and the tensile strength of PP/HDPE blends [11]. Formation of an OBC shell around dispersed HDPE particles reduced the particle size and was thought to improve interfacial adhesion.

Interfacial properties are not easily examined in the dispersed domain morphology of conventional melt blends. Microlayer coextrusion of many alternating layers of two polymers with individual layer thicknesses on the micron size scale creates a one-dimensional model of the melt blend [12]. Insertion of a tie-layer at each interface creates a one-dimensional model of the compatibilized blend [13]. Adhesion in microlayered polymers is conveniently studied with the T-peel test. Although peel tests generally do not supply absolute adhesive energies, the delamination toughness obtained from the test provides useful comparisons if the testing parameters are kept constant.

In the present study, we test the adhesion of two ethylene–octene statistical copolymers and a blocky copolymer to polypropylene and polyethylene using coextruded microlayered tapes. Adhesion is measured as delamination toughness and is compared for the various compatibilizers. The effects of tie-layer thickness, peel rate, and peel temperature on the adhesive properties of the different compatibilizers are examined.

2. Materials and methods

Microlayer tapes were coextruded using the three-component layer multiplying process described previously [14]. The tapes consisted of alternating layers of polypropylene (PP) and high density polyethylene (HDPE) separated by a tie-layer. The adherends and the tie-layers used in this study were provided by The Dow Chemical Company and are tabulated in Table 1. The adherends were a Ziegler–Natta polypropylene (PP), a Ziegler–Natta high density polyethylene (ZN-HDPE), and a metallocene-catalyzed high density polyethylene (m-HDPE). The tie-layers were two statistical ethylene–octene copolymers that differed in the comonomer content (EO855 and EO876), and an ethylene–octene multi-block copolymer (OBC) (Dow Experimental OBC). The EO855 had the same density as the OBC soft segment and the EO876 had approximately the same overall comonomer content and density as the OBC, Scheme 1. All the copolymers had about the same molecular weight, Table 1. Information regarding molecular weight, molecular weight distribution, comonomer content, and hard segment content was provided by The Dow Chemical Company.

Compression molded sheets with thickness of approximately 0.5 mm were prepared for thermal analysis and dynamic mechanical analysis. Pellets were sandwiched between Mylar® sheets, preheated at 190 °C under minimal pressure for 8 min and compressed at 10 MPa for 5 min in a Model 3912 Carver laboratory press, and quenched. Thermal analysis was performed with a Perkin–Elmer DSC-7 calorimeter under a nitrogen atmosphere. Specimens weighing 5–10 mg were cut from the molded sheets, and melting and cooling thermograms were obtained using a rate of 10 °C min^{-1}

Table 1
Materials

Material	Designation	C_8 content[a] (mol%)	Density (kg m^{-3})	M_w[a] (kg mol^{-1})	M_w/M_n[a]
Isotactic polypropylene	PP		900	340	4.6
Ziegler–Natta polyethylene	ZN-HDPE		961	120	9.6
Metallocene polyethylene	m-HDPE		960	110	2.1
Ethylene–octene statistical copolymer	EO855	17	855	220	2.1
Ethylene–octene statistical copolymer	EO876	11	876	220	2.0
Olefinic block copolymer	OBC	11	880	230	3.3

[a] Data provided by The Dow Chemical Company.

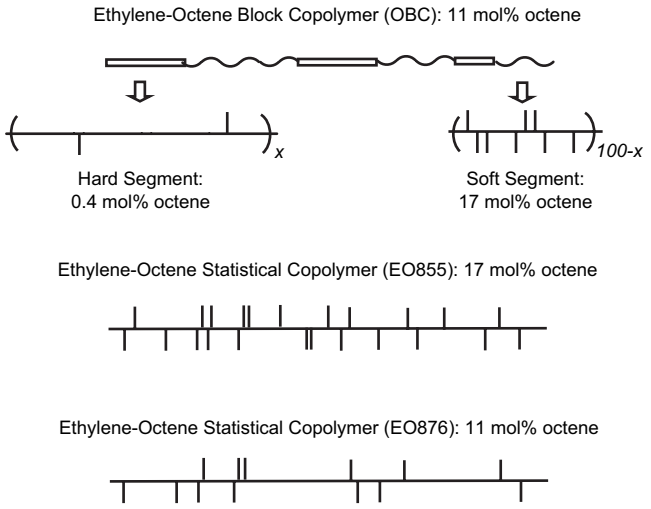

Scheme 1. Schematic representations of the ethylene–octene copolymer tie-layers.

from −60 to 190 °C. The percent crystallinity was calculated using a value of $\Delta H^o_m = 290$ J g^{-1} for the heat of fusion of 100% crystalline polyethylene. Dynamic mechanical thermal analysis (DMTA) was carried out with a Q800 Dynamic Mechanical Analyzer from TA Instruments. Specimens were tested in the dynamic tensile mode with a frequency of 1 Hz and a strain of 0.1% from −60 to 120 °C with a heating rate of 3 °C min^{-1} and a grip to grip distance of 13.0 mm.

Constrained uniaxial tensile stress–strain tests were performed on an MTS Alliance RT/30 testing machine at an engineering strain rate of 500% min^{-1}. Specimens having a highly constrained geometry in the width direction were cut from the compression molded sheets to have a thickness of 0.5 mm, a width of 80 mm, and a grip-to-grip separation of 20 mm. Engineering stress and strain were calculated conventionally from the initial cross-section area and grip separation.

Microlayered tapes with 65 layers (16 PP layers and 17 HDPE layers separated by 32 layers of the ethylene–octene tie-layer) were coextruded. The tapes were about 2 mm thick and 12 mm wide. Different tie-layer thicknesses were produced by varying the extruder feed ratios. The adherend PP and HDPE layers had thickness of about 50 μm, and the tie-layer thickness ranged from 1 to 15 μm. A microlayered tape of PP and HDPE with no tie-layer was also produced as a control. All the tapes were collected on a conveyor-belt take-off unit and quenched in cold water.

The microlayered tapes were microtomed at −70 °C through the thickness direction and normal to the extrusion direction to expose a cross-section of the layer interface. The cross-section was observed under an Olympus BH-2 optical reflection stereo microscope to determine layer uniformity and tie-layer thickness for the center adhesive layer. The microtomed cross-sections were imaged in a Digital Instruments Nanoscope IIIa atomic force microscope in the tapping mode.

Delamination was carried out with a modified T-peel test (ASTM D1876). Strips 6.4 mm wide and 20 cm long were cut from the center of the microlayered tape and notched by pushing a fresh razor blade into a tie-layer at the mid-plane of the tape. The notch was examined with an optical microscope to ensure that the crack started along a single interface. Tapes were subsequently loaded in an MTS Alliance RT/30 testing machine. To probe the effect of peel rate, specimens were peeled at 0.1, 1, 10, 100, and 1000 mm min^{-1} at ambient temperature. To probe the effect of peel temperature, specimens were peeled at temperatures between −60 and 90 °C at a rate of 10 mm min^{-1} in an Instron 3119 environmental chamber cooled with liquid nitrogen. Tapes were held at temperature for 20 min before testing. At least

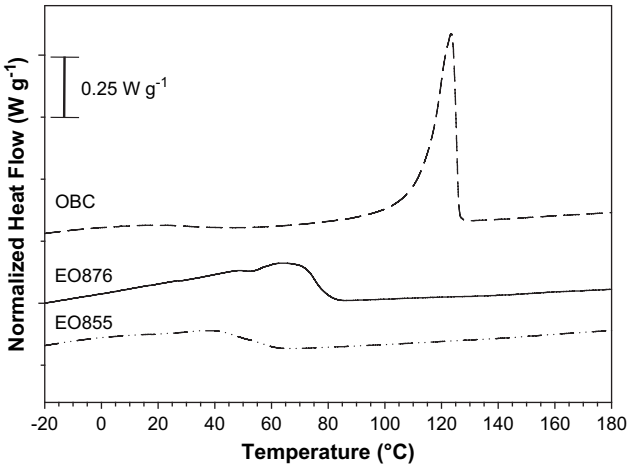

Fig. 1. Heating thermograms of the tie-layer copolymers obtained with a heating rate of 10 °C min^{-1}.

two specimens of each composition were tested at each temperature and rate.

The crack tip damage zone was too small for in situ observation during the peel test with conventional photography. Instead, the damage zone was imaged under an Olympus BH-2 microscope. Specimens were illuminated in the reflection mode, and images were captured while the sample was peeled by hand at approximately 10 mm min^{-1}.

Composition of the matching peel surfaces was determined by a Nicolet 800 FTIR spectrometer in the ATR mode. Five different areas on each peel surface were tested. The matching surfaces were coated with 100 Å of gold and examined in a JEOL 840-A scanning electron microscope (SEM).

3. Results and discussion

3.1. Thermal characterization of copolymers

Thermograms for the three copolymers used in the study are shown in Fig. 1. The statistical copolymers exhibited broad melting endotherms with maxima at 38 and 64 °C for EO855 and EO876, respectively. The higher melting temperature and larger melting enthalpy of EO876, compared to EO855, were due to the lower comonomer content. In contrast to the statistical copolymers, the OBC showed a sharp melting endotherm with peak temperature at 123 °C. Although OBC and EO876 had about the same total comonomer content and about the same total crystallinity, the difference in melting behavior reflected the organized, lamellar crystals of the long crystallizable hard segments of OBC compared to the primarily fringed micellar crystals of the statistically distributed crystallizable segments in EO876. The soft segment of OBC was similar to EO855 in density and octene content, and a very weak and broad maximum in the temperature range of the EO855 melting peak was discerned in the thermogram of OBC. The thermal properties of the copolymers are summarized in Table 2.

Table 2
Selected thermal properties

Material	ΔH^a (J g^{-1})	X_c (%)	T_m (°C)	T_c (°C)	T_g (°C)	T_α (°C)
PP	103	50	165	123	18	73
ZN-HDPE	223	77	137	114		54
EO855	9	3	38	45	−39	–
EO876	37	13	64	44	−32	–
OBC	39	13	123	98	−42	76

[a] DSC enthalpy values are from first heating.

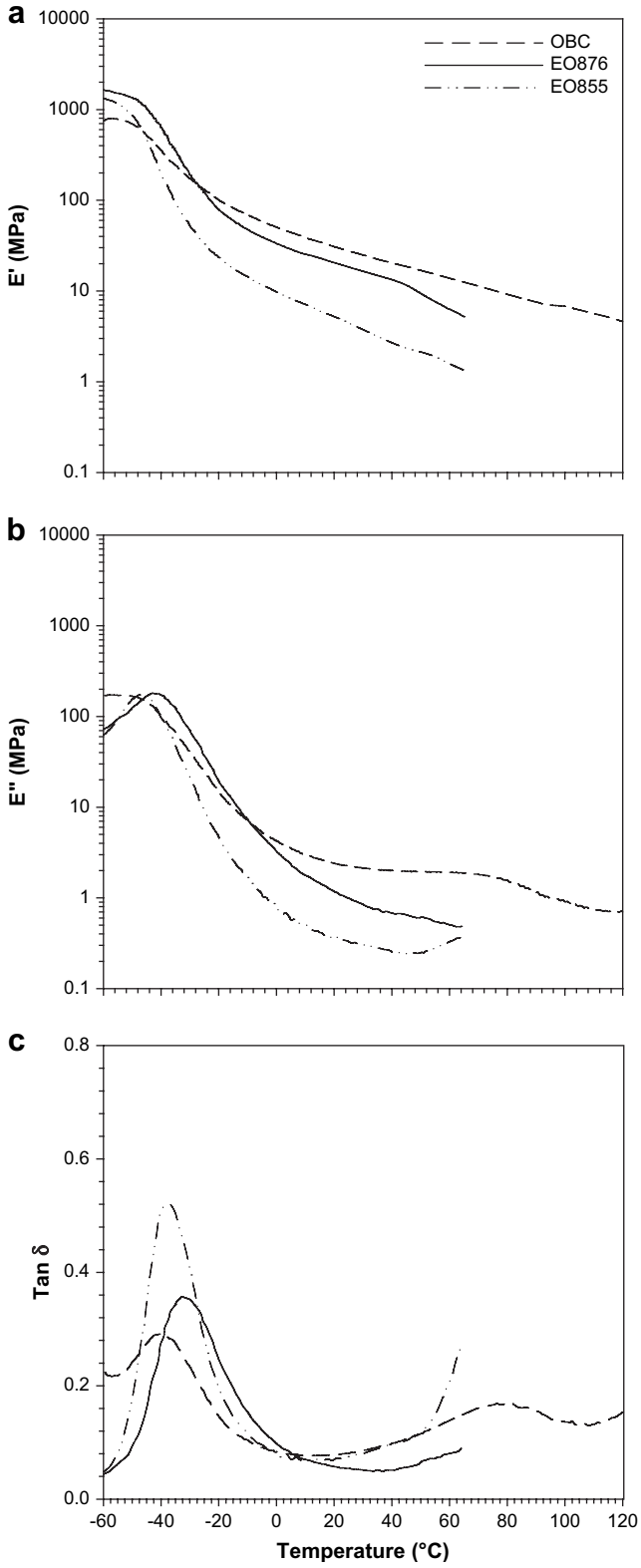

Fig. 2. DMTA spectra of the tie-layer copolymers: (a) E'; (b) E''; and (c) tan δ.

The dynamic mechanical behavior of the copolymers is shown in Fig. 2. All the copolymers exhibited a β-relaxation peak that was accompanied by a substantial drop in E'. The peak temperature in tan δ was taken as the glass transition temperature T_g. The peak intensity and drop in E' were largest in EO855, which had the lowest crystallinity. Increasing the comonomer content of the statistical copolymer had the effect of increasing the relaxation

intensity and decreasing the relaxation temperature somewhat, Table 2. Although EO876 and OBC had about the same crystallinity, the blocky comonomer distribution of OBC resulted in slightly lower relaxation intensity and a decrease of about 10 °C in T_g. Above ambient temperature, the curves for the statistical copolymers terminated with a rapid increase in tan δ that marked the onset of melting. In contrast, the OBC exhibited the α-relaxation at about 75 °C in both tan δ and E''. The α-relaxation is associated with coupled motion of crystalline and amorphous chain segments. The fringed micellar crystals of the statistical copolymers were not stable enough to support these motions. Before the α-relaxation motions were activated, melting started, which resulted in loss of the elastomeric network that the fringed micellar junctions provided. In contrast, the substantially higher melting temperature of the more stable OBC lamellar crystals allowed for the α-relaxation motions.

3.2. Delamination in microlayered tapes

Optical micrographs of the microlayered tapes clearly revealed the layered structure. The tie-layer thickness ranged from 1 to 15 μm; Fig. 3 shows examples with relatively thin and relatively thick OBC tie-layers. The interfaces between the tie-layer and the PP layer (darker layer) and between the tie-layer and the HDPE layer (lighter layer) were sharp and clearly visible.

The tape was notched at one end by driving a razor blade into the adhesive layer. When the notched specimen was loaded, the arms bent into the T-peel configuration as the load gradually increased until the crack started to propagate steadily at a constant load. Plastic deformation of the beam arms was evident because the beam arms did not return to their original shape upon removal of the load and the curvature of the beam arms did not match the elastica prediction [15,16].

The peeled surfaces were probed with ATR-FTIR in order to identify the failure location. Correspondence of the spectrum from one surface to that of the adhesive copolymer and correspondence of the spectrum from the matching surface to that of PP, Fig. 4, confirmed that the tie-layer delaminated cleanly from the PP layer. A trace of HDPE detected in the tie-layer spectrum was attributed to the diffusion of low molecular weight HDPE fractions into the tie-layer.

The delamination toughness G was obtained from the constant load P measured during crack propagation and the specimen width W as ($G = 2P/W$). The effect of tie-layer thickness on the delamination toughness measured at a 10 mm min^{-1} peel rate and 21 °C is shown in Fig. 5. The delamination toughness of OBC was substantially higher than that of EO855, which had the same composition as the OBC soft segment, and was also much higher than that of EO876, which had the same comonomer content and crystallinity as OBC. Clearly, the blocky nature of OBC was responsible for the higher delamination toughness compared to the statistical copolymers.

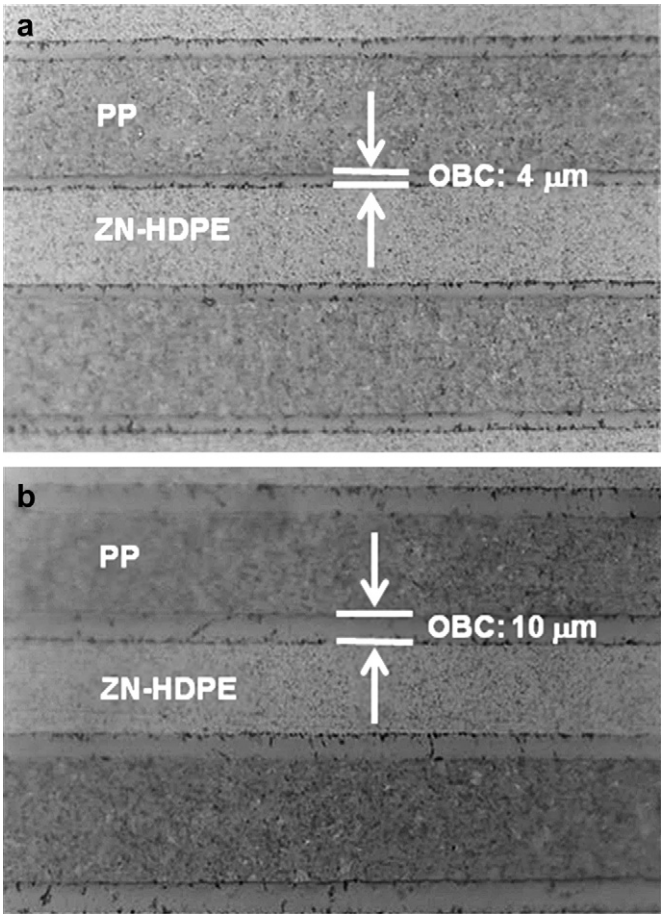

Fig. 3. Optical micrographs showing the layered structure of the microlayered tapes: (a) A tape with 4 μm OBC layers; and (b) a tape with 10 μm OBC layers.

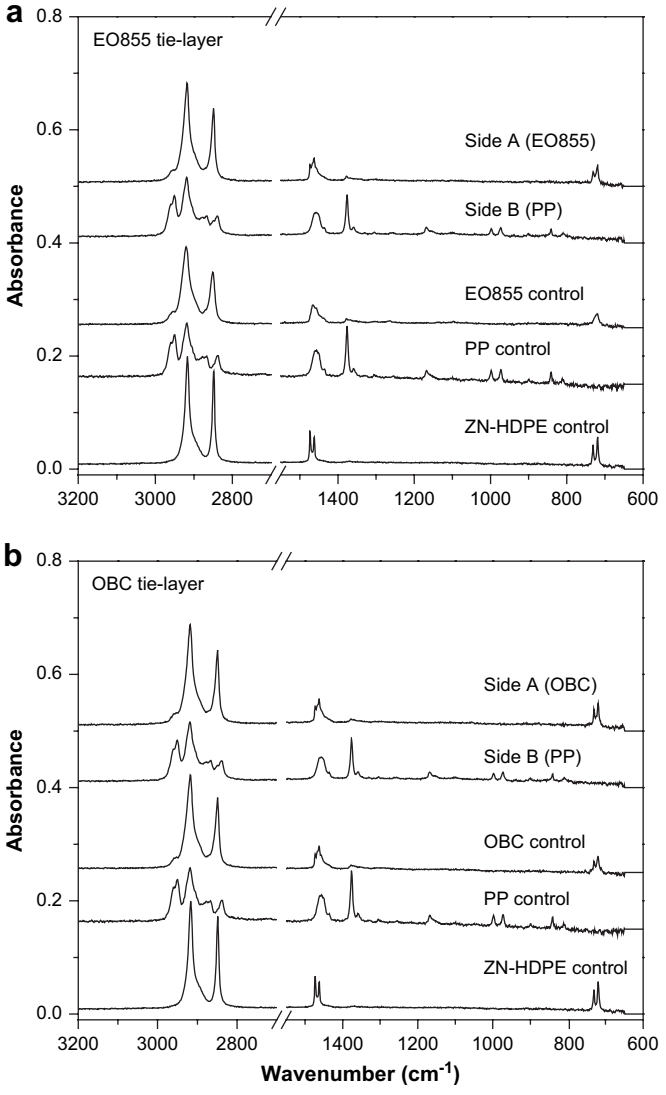

Fig. 4. FTIR spectra of matching peel fracture surfaces compared with spectra of the tape constituents.

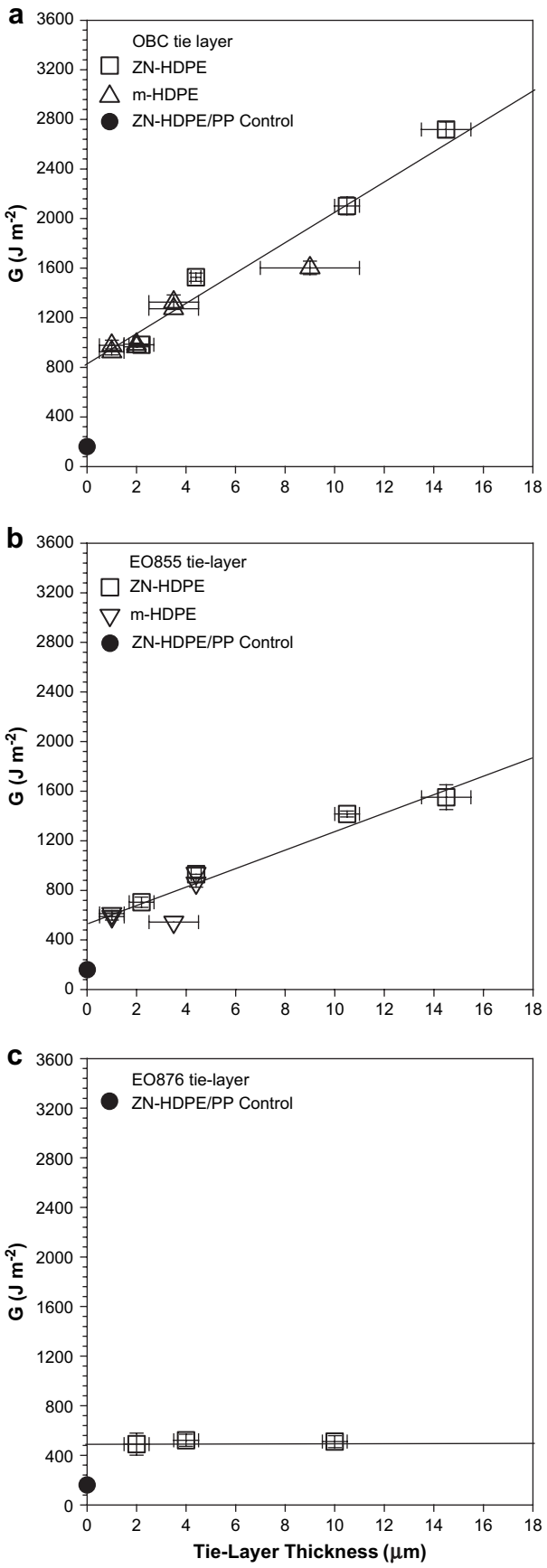

Fig. 5. The effect of tie-layer thickness on the delamination toughness: (a) OBC; (b) EO855; and (c) EO876.

The delamination toughness increased linearly with layer thickness for OBC and EO855, indicating that energy was absorbed by the deformation of the entire tie-layer thickness. Extrapolation to zero tie-layer thickness gave a value for OBC that was approximately twice that of EO855. The extrapolated values were significantly higher than the delamination toughness measured for PP/HDPE tapes without a tie-layer. The extrapolated values presumably combined the contributions of adhesive failure and beam arm deformation. The beam arm deformation consisted of two components, stretching and bending. In similar peel tests using microlayered tapes, both contributions were found to be within the experimental error [17]. Therefore, adhesive failure and tie-layer deformation were the major factors controlling delamination toughness. The adhesive contribution was reflected in the extrapolated value of delamination toughness and the slope provided the contribution of tie-layer deformation.

For EO876, the delamination toughness was independent of the tie-layer thickness over the range of thicknesses tested with a value close to the extrapolated value for EO855. In this case, either tie-layer deformation was limited to a small and constant region adjacent to the polypropylene interface, or the contribution of tie-layer deformation was negligible compared to other contributions to the delamination toughness.

The incompatible interface between a semicrystalline polymer and a soft viscoelastic thermoplastic can exhibit unexpectedly high delamination toughness due to the formation of crystalline influxes [18,19]. The influxes provide sufficient connectivity to support viscoelastic–plastic deformation of the soft layer. The delamination toughness in this case is given as [20]

$$G = \beta\frac{\sigma_c^2}{2E}h + G_{1c} \tag{1}$$

where h is the effective deformed layer thickness, E is the temperature and rate sensitive tensile modulus of the soft layer, σ_c is the critical peel stress developed at the interface, and β is the fraction of the stored elastic energy density that is dissipated by deformation of the soft layer. The first term in Eq. (1) represents the energy dissipated in the soft layer and the second term is the true interface strength due to the influxes.

The value of h was taken as the layer thickness for OBC and EO855 based on the linear relationship between G and h. The slope of the plots in Fig. 5a and b gives $\beta(\sigma_c^2/2E)$ as 122 MPa for OBC and 75 MPa for EO855. Furthermore, the term $\beta(\sigma_c^2/2E)$ can be expressed as $\beta(\sigma_c\varepsilon_c/2)$ where ε_c is the critical strain at the crack tip and $\varepsilon_c = (\sigma_c/E)$. Assuming that $\beta = 1$ and taking ε_c as 1100% for OBC and 1700% for EO855 from direct measurements of the crack tip

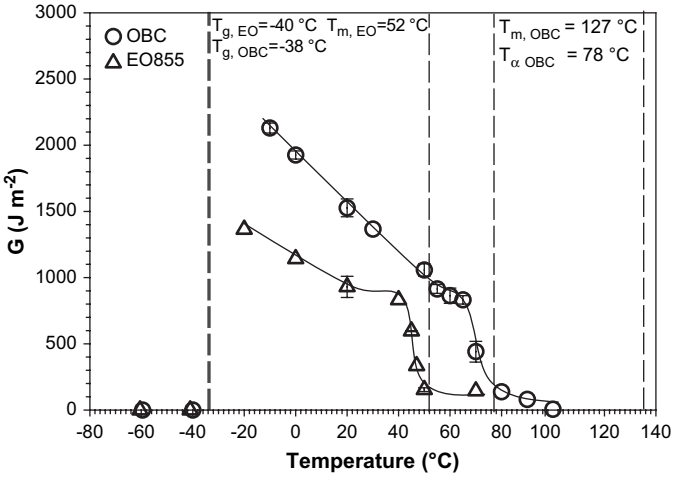

Fig. 6. Effect of temperature on the delamination toughness of OBC and EO855.

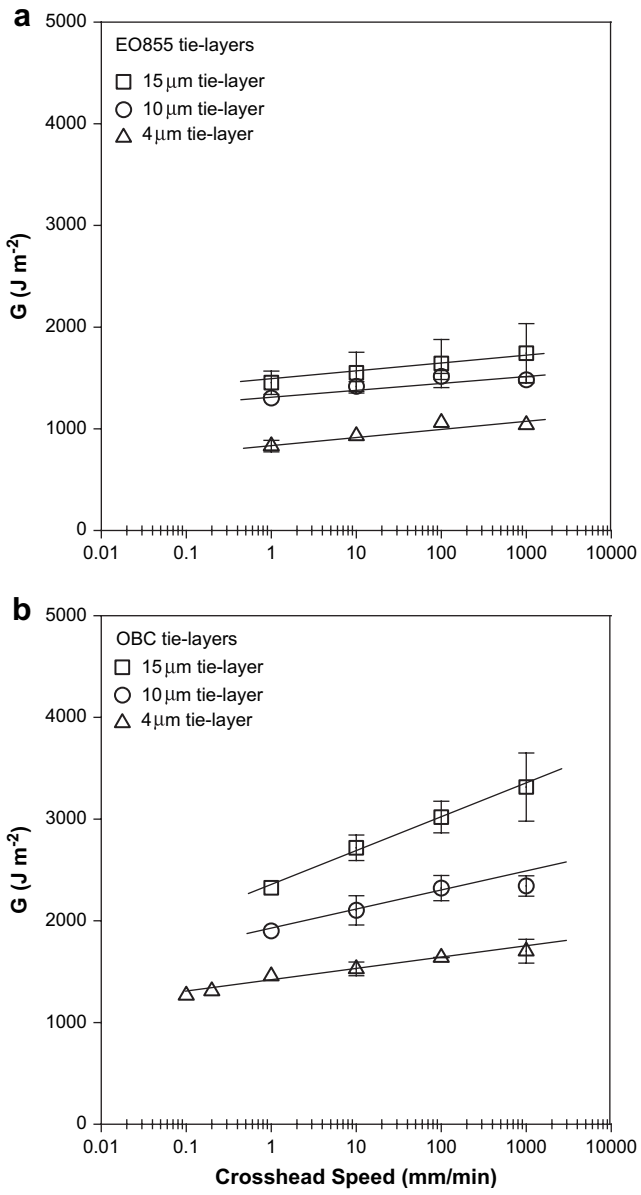

Fig. 7. Effect of peel rate on the delamination toughness of OBC and EO855 at 21 °C.

strain in the deformed layer, σ_c is 22 MPa for OBC and 8.8 MPa for EO855. The corresponding values of E are 2 MPa for OBC and 0.5 MPa for EO855. These values are reasonable [19]. However, the linear assumption probably underestimates the area under the stress–strain curve and leads to slightly high values of σ_c.

Peel tests of tapes made with a narrow molecular weight metallocene HDPE (m-HDPE) and a broader molecular weight ZN-HDPE revealed no significant differences in the delamination toughness (Fig. 5a and b). Thus, only the ZN-HDPE tapes were investigated further. The effect of the temperature on the delamination toughness measured at a 10 mm min^{-1} peel rate on tapes with 4 μm OBC and EO855 tie-layers is shown in Fig. 6. Below T_g of the tie-layer, all the tapes failed before the beam arms were able to adopt the T-peel configuration. The interface between the tie-layer and the polypropylene layer failed catastrophically without achieving stable crack propagation. Above T_g, the tie-layers provided very strong adhesion. The delamination toughness decreased steadily as the temperature increased reflecting the temperature dependence of σ_c^2/E in Eq. (1). At a higher temperature, a transitional drop in G to almost zero occurred over a small change in temperature. The transition temperature was substantially lower for EO855, 40–50 °C, than for OBC, 70–80 °C. The transition temperature corresponded to T_m of the statistical copolymer and to T_α of the OBC. Above the transition temperature, failure occurred cohesively through the tie-layer due to softening of the crystalline phase.

Increasing peel rate generally has the same effect on delamination toughness as decreasing peel temperature [21]. Fig. 7 shows the logarithmic dependence of delamination toughness on the peel rate at 21 °C. In all cases, the tie-layer delaminated cleanly from the PP layer. In tapes with EO855 tie-layers, the delamination toughness increased approximately 20% when peel rate was increased from 1 to 10^3 mm min^{-1} regardless of the tie-layer thickness. The rate dependence was greater for tapes with OBC. Over the same range in peel rate, the delamination toughness increased about 30% for tapes with 4 μm OBC tie-layers and 60% for tapes with 10 μm OBC tie-layers. The larger rate dependence of delamination toughness in tapes with OBC tie-layers was consistent with the stronger temperature dependence in the regime between T_g and the transitional drop (see Fig. 6).

3.3. Delamination mechanism

Viewing the propagating crack tip from the side under a stereoscopic reflection microscope revealed the deformation zone in the tie-layer that preceded interfacial adhesive failure. Fig. 8 shows

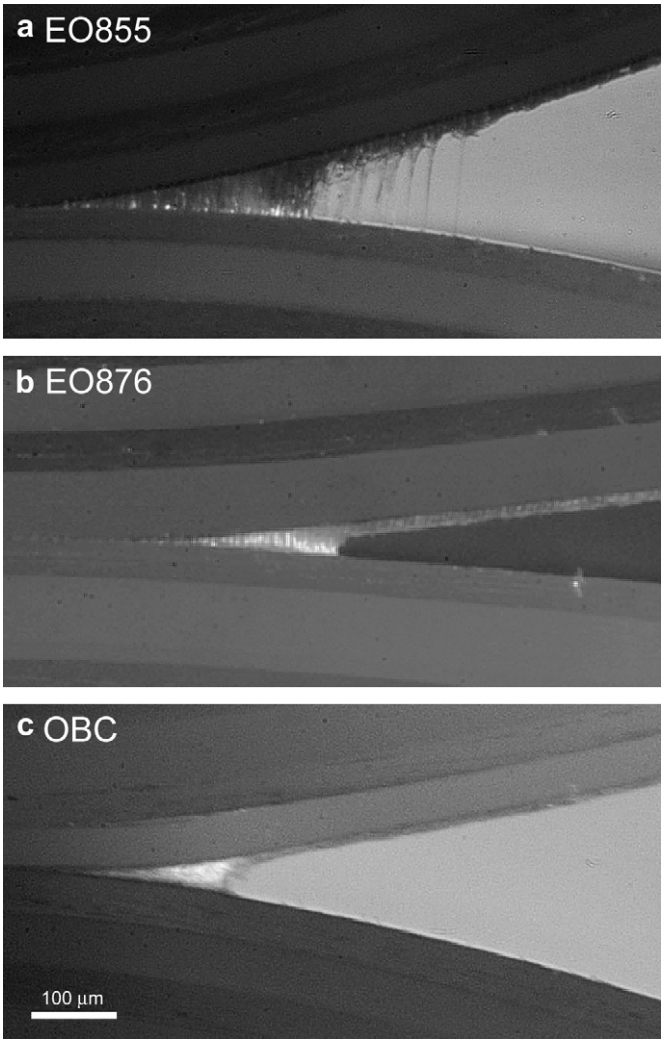

Fig. 8. Optical micrographs of the crack tip damage zone of 4 μm tie-layers: (a) EO855; (b) EO876; and (c) OBC.

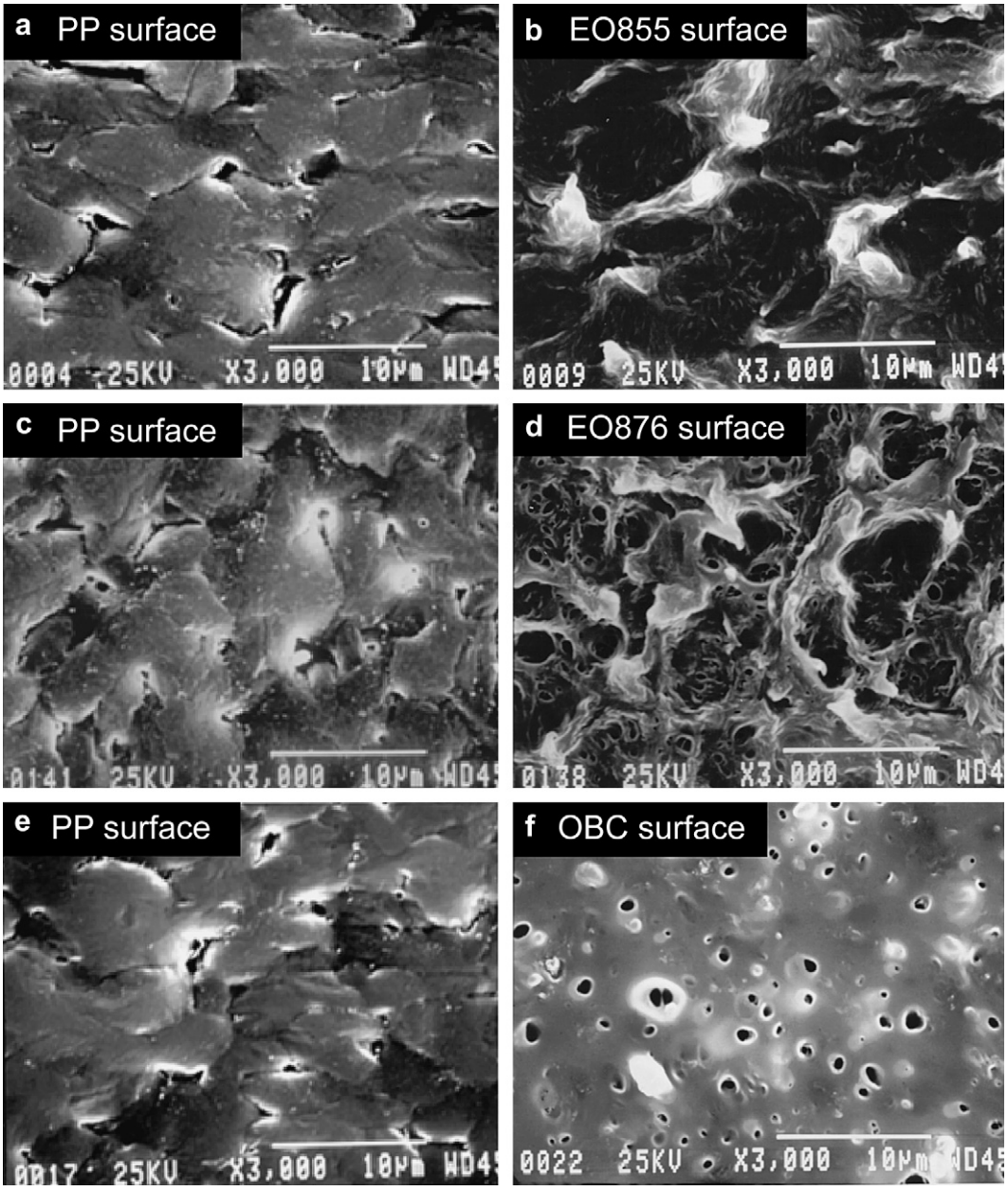

Fig. 9. SEM images of matching peel fracture surfaces obtained at 21 °C.

the results for 4 μm tie-layers. The EO855 tie-layer produced a very large and highly fibrillated damage zone. The highly stretched fibrils snapped back upon separation from the PP layer. The damage zone of EO876 was also fibrillated, but was much smaller than that of EO855. The damage zone of OBC was considerably smaller than that of EO855 and comparable in size to that of EO876. However, the shape and texture were much different. The OBC damage zone did not exhibit fibrillation. Rather, it was smooth and featureless. Pronounced sucking-in at the free crack tip surface indicated plastic deformation. Cavitation was also a possibility, although this could not be confirmed. Furthermore, the angle of the crack tip opening was much larger than that of EO876, which reflected the higher peel force required to propagate the crack. The dimensions of the damage zone increased in proportion to the tie-layer thickness for EO855 and OBC, which was consistent with deformation of the entire tie-layer.

The SEM images of matching tie-layer and PP surfaces of peeled tapes are shown in Fig. 9. The EO855 surface was characterized by numerous short fibrils. The matching PP surface showed cavities with about the same spacing as the fibrils on the EO surface. Indeed, the spacing of the EO fibrils and the PP cavities was on the size scale of the PP spherulite diameter, about 5 μm. Similar features have been observed by others on delaminated surfaces from PP/HDPE sandwich structures. Bartzak and Galeski were the first to attribute this phenomenon to the influx of HDPE into the interstices of PP spherulites during crystallization of the latter [18]. It was believed that the volume contraction that accompanied PP crystallization caused a vacuum that trapped molten HDPE before the HDPE solidified. Because of the way they form, the number and length of the influxes depend on the thermal history, including the melt temperature at which the interface forms, the cooling rate from the melt and any subsequent annealing steps. The influxes are thought to be responsible for the higher than theoretically predicted delamination force measured for the PP/HDPE interface. Calculations by Wool suggested that fibrillation of the influxes during delamination could account for the interfacial strength [19,20].

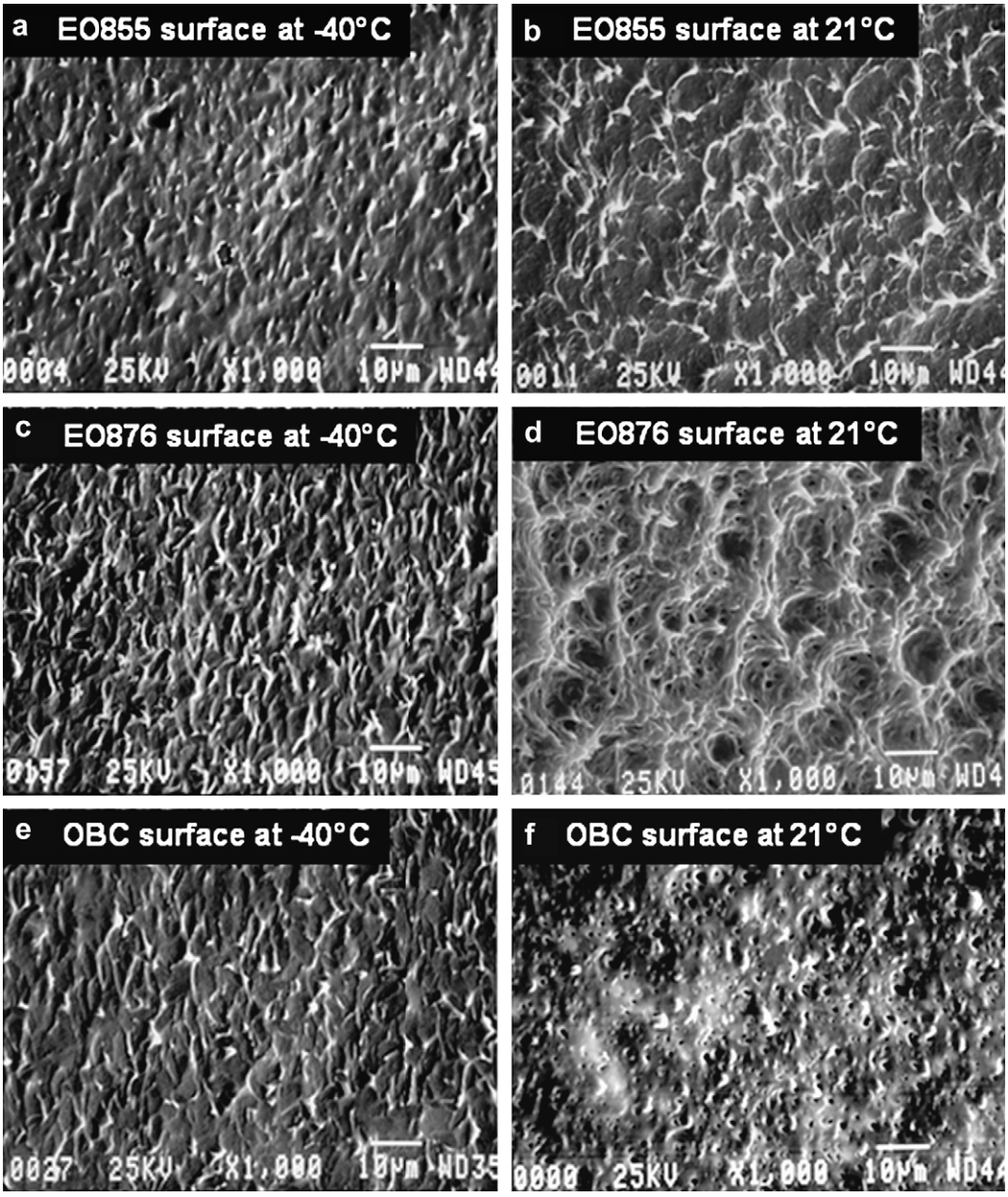

Fig. 10. Comparison of tie-layer fracture surfaces obtained at −40 and 21 °C. The tilt angle was 40°.

All the PP surfaces exhibited voids that were left when the tie-layer influxes were fractured or pulled out during final separation of the interface. It appeared that all the tie-layers flowed into the interspherulitic cavities of the crystallizing PP to form an interdigitated interface. On the other hand, features on the tie-layer surface differed among the several copolymers. The surfaces of the statistical copolymers contained evidence of fibrillation, which was consistent with the appearance of the crack tip damage zones. Correspondence in the diameter and spacing as the holes on the PP surface and the fibrils on the EO855 surface suggested that the fibrils were anchored by interdigitation with the PP surface. The EO876 surface exhibited more profuse fibrillation and cavitation than the EO855 surface, even though EO876 had lower delamination toughness than EO855. The apparent difference in the amount of damage probably reflected the extent to which the deformed tie-layer recovered after final separation. Thus, the less elastic EO876 tie-layer would not have recovered as much as the EO855 tie-layer. Whereas both the EO surfaces showed fibrillation as the primary damage mechanism, the OBC surface was quite different. Instead of fibrils, there were numerous cavities of approximately 1 μm. Otherwise, the surface was largely featureless.

In order to obtain tie-layer surfaces with minimal deformation, specimens were peeled at −40 °C, below the T_g of the tie-layer where the interface fractured catastrophically in a brittle manner. The −40 °C PP surfaces were indistinguishable from the 21 °C PP surfaces in Fig. 9; they all exhibited voids that were left when the tie-layer influxes were fractured or pulled out during final separation of the interface. The −40 and 21 °C tie-layer fracture surfaces are compared in Fig. 10. The lower magnification and 40° tilt angle of these images best revealed the fibrillated structure of the tie-layer. The −40 °C EO855 surface contained about the same density of fibrous entities as the 21 °C surface, however, the fibrils were not as highly drawn as on the 21 °C surface. The appearance of fibrous entities on the −40 °C surface was consistent with their origin as interdigitated influxes. Possibly, contraction of the influxes and loss of tie-layer ductility at the T_g facilitated influx pullout without the

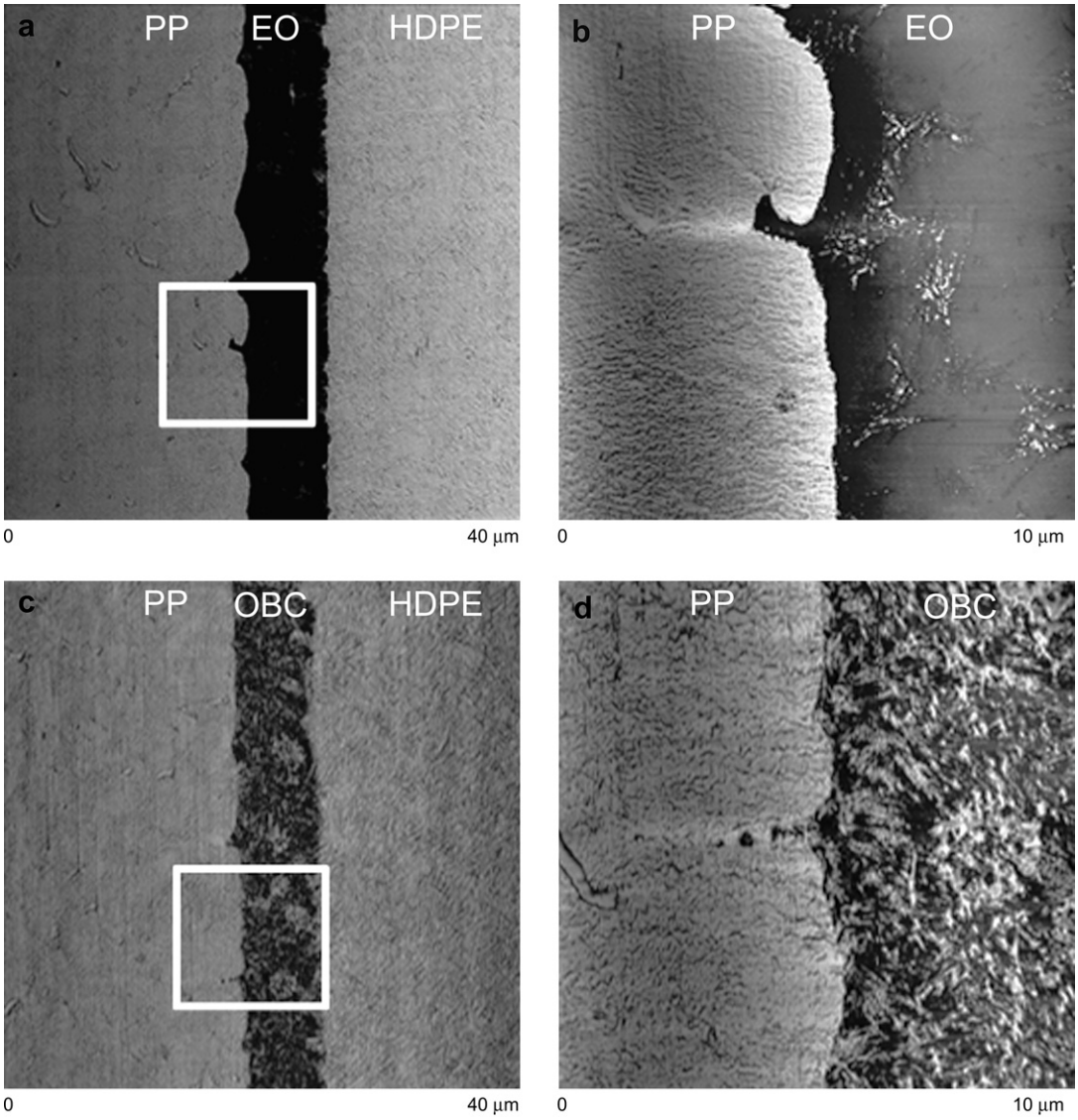

Fig. 11. AFM phase images of the interface: (a) The EO855 tie-layer; (b) higher resolution of the EO855/PP interface; (c) the OBC tie-layer; and (d) higher resolution of the OBC/PP interface.

energy-absorbing fibrillation processes that provided adhesive strength at temperatures above the tie-layer T_g. The −40 °C surfaces of EO876 and OBC were essentially indistinguishable from that of EO855. The presence of fibrils on the surface when the delamination toughness was essentially negligible provided further confirmation that all the tie-layers formed an interdigitated interface.

The lower magnification, tilted images of the 21 °C surfaces further emphasized the differences among the three tie-layers. In addition to the numerous cavities on the OBC surface, the image revealed the presence of some short fibrils. The short fibrils had about the same size and spacing as the fibrils on the −40 °C OBC surface. The fibrils probably resulted from fracture or pullout of interdigitated influxes, suggesting that the influxes served to anchor the tie-layer. However, it was also apparent that the major contribution to energy absorption in the OBC tie-layer did not come from fibrillation, but from some other deformation mechanism.

Direct visualization of the influxes was sought by examining the interface between the PP layer and the tie-layer with AFM. The cross-section of a typical EO855 tie-layer is shown in Fig. 11a and b. The lower resolution image shows the tie-layer between PP (left side) and HDPE (right side). The undulating periodicity along the PP/EO855 interface was attributed to the boundaries of PP spherulites. The spherulites ranged from 2 to 5 μm in diameter. In addition to the periodic spherulitic boundaries, there were more acute interdigitated features such as the "boot-shaped" one shown in the higher resolution image. The diameter of the influxes was on the same size scale of approximately 1–3 μm as the fibrils seen on the peel fracture surfaces. The bundles of lamellae in EO855 layer were thought to be HDPE fractions that diffused into the tie-layer during melt processing. The EO855 itself formed fringed micellar crystals.

The cross-section of an OBC tie-layer is shown in Fig. 11c and d. The lamellar texture of the OBC contrasted with the featureless appearance of the EO855 tie-layer. The interfacial features were similar to those of the EO855 tie-layer with an undulating periodicity along the PP/EO855 interface that was attributed to the boundaries of PP spherulites. In this case, the higher resolution image showed an influx that was straight, in contrast to the "boot-shape" of the EO855 influx. The shape of the influx was highly dependent on the microtome cut and angle, and only a few influxes were imaged. Although the "boot-shaped" influxes were only observed on the PP/EO855 interface and not on the PP/OBC interface, the number of influxes imaged was too small to claim that the "boot shape" was unique to the PP/OBC interface.

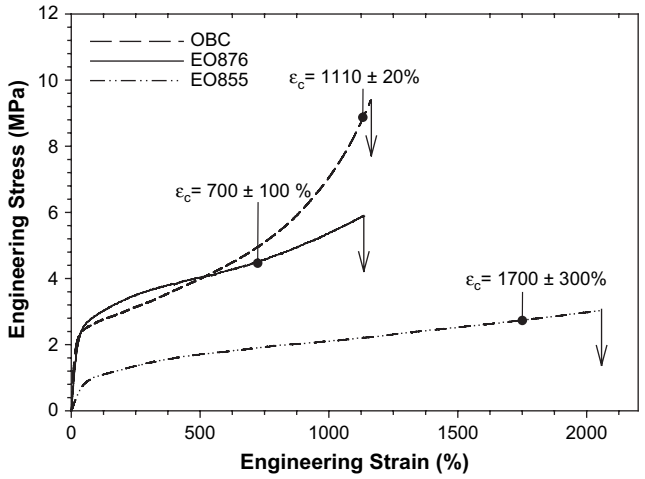

Fig. 12. Constrained stress–strain curves of the tie-layer copolymers. The solid symbols indicate the maximum strain in the peel damage zone ε_c.

It is now interesting to speculate about why the blocky structure of OBC imparts significantly higher delamination toughness than the statistical comonomer distribution of EO855 and EO876. Contributions come from interspherulitic influxes and from intraspherulitic entrapment of entangled tie-layer chains in the polypropylene spherulite. Assuming that the influxes are sufficiently interlocked that they fracture rather than pullout, delamination toughness should reflect the cohesive fracture stress of the tie-layer. Constrained uniaxial stress–strain curves for the tie-layers are presented in Fig. 12. The initial response reflected the amount of crystallinity. Thus, OBC and EO876 had about the same modulus and yield stress, whereas the values for EO855 were much lower. The differences between the statistical and blocky copolymers appeared at higher strains. Neither EO876 nor EO855 exhibited strong strain-hardening, whereas pronounced strain-hardening of OBC resulted in the highest fracture stress. The maximum strain in the tie-layer ε_c was estimated from the initial thickness of the tie-layer and the maximum extension of the tie-layer in the crack tip damage zone. The resulting strain in the tie-layer at final separation is indicated on Fig. 12 for the 4 μm tie-layers. The toughness, taken as the area under the stress–strain curve up to the maximum tie-layer strain, was about the same for the two statistical copolymers, and was substantially higher for the blocky copolymer. Although the loading conditions in the constrained uniaxial test and in the peel test were somewhat different, qualitatively the results from the stress–strain curves correlated well with the measured delamination toughness.

Although mechanical entrapment is thought to be more important, the contribution of intraspherulitic entrapment may be significant especially if entanglement loss by relaxation is minimized by rapid cooling [18]. With higher comonomer content than EO876, it is anticipated that OBC soft segment and EO855 chains will be more compatible with PP and will form more interfacial bridges. This is consistent with OBC and EO855 both having higher delamination toughness than EO876. Considering next the higher delamination toughness of OBC compared to EO855, it seems unlikely that EO855 would form more bridges at the melt temperature than OBC soft segments, even if the OBC soft segments were preferentially located at the PP interface. However, it can be imagined that the rapid crystallization of OBC hard segment prevents disentanglement of soft segment bridges whereas the lower crystallization temperature of EO855 allows more time for relaxation [18]. Thus, in the final condition, the OBC may have more bridges across the interface than EO855. Thus, consideration of both interspherulitic influxes and intraspherulitic entrapment is consistent with higher delamination toughness for the blocky copolymer. Indeed, both factors may contribute to adhesion of the tie-layer to PP.

4. Conclusions

The study examined some ethylene copolymers as candidate tie-layers for adhering polypropylene and polyethylene. The tie-layer thickness was readily controlled by coextruding microlayered tapes with many alternating layers of polypropylene and polyethylene each separated by a thin tie-layer. In the T-peel test used to determine the delamination toughness, failure was preceded by a highly deformed damage zone in the tie-layer. Final separation occurred at the interface between the tie-layer and polypropylene. The delamination toughness of a blocky copolymer was significantly higher than that of a statistical copolymer which had the same composition as the soft blocks of the blocky copolymer, and was also substantially higher than that of a statistical copolymer which had the same comonomer content and crystallinity as the blocky copolymer. Clearly, the blocky nature was responsible for the higher delamination toughness compared to the statistical copolymers. Contributions from interspherulitic influxes and from intraspherulitic entrapment of entangled tie-layer chains in the polypropylene spherulite were considered. Both were consistent with higher delamination toughness of the blocky copolymer, however, it is generally thought that mechanical entrapment is more important. Assuming that the influxes fractured rather than pulled out, higher tensile strength of OBC provided for higher delamination toughness. In addition, the OBC retained significant delamination toughness to 70–80 °C whereas the statistical copolymer lost delamination toughness at a lower temperature of 40–50 °C. The transition temperature corresponded to T_α of the OBC and to T_m of the statistical copolymer. The fringed micellar crystals of the statistical copolymers were not stable enough to support the α-relaxation motions. Before the α-relaxation motions were activated, melting resulted in loss of the elastomeric network that the fringed micellar junctions provided.

Acknowledgement

The authors thank The Dow Chemical Company for generous technical and financial support.

References

[1] Robertson RE, Paul DR. J Appl Polym Sci 1973;17:2579–95.
[2] Stehling FC, Huff T, Speed S, Wissler G. J Appl Polym Sci 1981;26:2693–711.
[3] Bartlett DW, Barlow DW, Paul DR. J Appl Polym Sci 1982;27:2351–60.
[4] Ha CS. J Appl Polym Sci 1989;37:317–34.
[5] Blom HP, Teh JW, Rudin A. J Appl Polym Sci 1996;61:959–68.
[6] Souza AMC, Demarquette NR. Polymer 2002;43:3959–67.
[7] Vranjes N, Rek V. Macromol Symp 2007;258:90–100.
[8] Creton C, Kramer EJ, Hadziioannou G. Macromolecules 1991;24:1846–53.
[9] Creton C, Kramer EJ, Hui CY, Brown HR. Macromolecules 1992;25:3075–88.
[10] Arriola DJ, Carnahan EM, Hustad PD, Kuhlman RL, Wenzel TT. Science 2006; 312:714–9.
[11] Chen HY, Poon B, Chum SP, Dias P, Hiltner A, Baer E. ANTEC 2007 Soc Plast Eng Conf Proc; 2007. p. 1201–5.
[12] Poon BC, Chum SP, Hiltner AH, Baer E. Polymer 2004;45:893–903.
[13] Ebeling T, Hiltner A, Baer E. J Appl Polym Sci 1998;68:793–805.
[14] Bernal-Lara TE, Ranade A, Hiltner A, Baer E. Nano- and microlayered polymers: structure and properties. In: Michler GH, Balta Calleja FJ, editors. Mechanical properties of polymers based on nanostructure and morphology. Boca Raton: CRC Press; 2005. p. 629–81.
[15] Ebeling T, Hiltner A, Baer E. Polymer 1999;40:1985–92.
[16] Kendall K. J Adhes 1973;5:105–17.
[17] Ronesi V, Cheung YW, Hiltner A, Baer E. J Appl Polym Sci 2003;89:153–62.
[18] Bartczak Z, Galeski A. Polymer 1986;27:544–8.
[19] Wool RP. Polymer interfaces: structure and strength. New York: Hanser; 1995 [chapter 10].
[20] Wool RP. In: Chaudhury M, Pocius AV, editors. Diffusion and autohesion. Adhesion science and engineering, vol. 2. Amsterdam: Elsevier; 2002. p. 371–6.
[21] Ebeling T, Hiltner A, Baer E. Polymer 1999;40:1525–36.